Passive Acoustic Metasurface with Unitary Reflection Based on Nonlocality

Li Quan and Andrea Alù

Phys. Rev. Applied **11**, 054077 — Published 28 May 2019

DOI: 10.1103/PhysRevApplied.11.054077

Passive Acoustic Metasurface with Unitary Reflection Based on Nonlocality

Li Quan[1] and Andrea Alù[1,2,3,4*]

[1]*Department of Electrical and Computer Engineering, The University of Texas at Austin, Austin, Texas 78712, USA*

[2]*Photonics Initiative, Advanced Science Research Center, City University of New York, New York, NY 10031, USA*

[3]*Physics Program, Graduate Center, City University of New York, New York, NY 10026, USA*

[4]*Department of Electrical Engineering, City College of New York, New York, NY 10031, USA*

[*]To whom correspondence should be addressed (email: aalu@gc.cuny.edu)

Metasurfaces have introduced large flexibility in manipulating the impinging wavefront for light and sound by locally engineering the reflection and transmission coefficients based on generalized Snell's laws. Local phenomena in each unit cell, however, are fundamentally limited in the level of efficiency with which anomalous wavefront transformations can be achieved. Here, we explore acoustic metasurfaces with suitably engineered nonlocality, obtained by coupling neighboring cells. We demonstrate that nonlocal passive metastructures can overcome the limitations of local designs, and mimic balanced gain and loss distributions, enabling unitary efficiency for extreme beam steering.

I. Introduction

[*] Corresponding author: aalu@gc.cuny.edu

Single-layered low-profile artificial surfaces have attracted significant attention recently, due to their capability of manipulating the impinging wave, over a compact design and moderate fabrication complexity compared with bulky metamaterial devices. These metasurfaces have shown interesting prospects for applications in communications, imaging, medical devices, both for electromagnetic and acoustic waves [1]-[5]. Early examples of metasurfaces were mainly based on accurately controlling the local reflection and/or transmission properties of each unit cell, so that the impinging wave can acquire an additional tangential momentum necessary to redirect the incoming energy towards the desired direction, dubbed phase-gradient metasurfaces for electromagnetics [6]-[10] and acoustics [11]-[14]. More recent studies have highlighted inherent efficiency limitations in these designs, since phase-gradient metasurfaces neglect impedance matching constraints and are therefore not able to redirect all incident energy into the desired direction, with a portion of the impinging wave going into unwanted parasitic diffraction orders [15]-[17]. The efficiency decreases rapidly as the steering angle deviates from specular reflection, and hence a clear trade-off exists between efficiency and extreme wavefront transformations in conventional gradient metasurfaces. More recently, Huygens metasurfaces have been introduced, in which a careful design of the local impedance along the surface and the addition of bianisotropic phenomena have ensured unitary efficiency for arbitrary wave steering, both for electromagnetic [18]-[20] and acoustic [21]-[22] waves. However, unitary efficiency for reflective metasurfaces still requires the use of active materials, which makes the realization challenging [15]. These findings raise the important question of whether it is possible to realize ideal anomalous wave steering with passive metasurfaces.

In [15]-[17] it was noticed that a single ultrathin surface can generally achieve unitary steering efficiency only provided that, while it is globally lossless, it has an impedance profile with local

regions of gain and loss. It was further suggested that one way to create this impedance profile is to induce nonlocality, which may drive energy from one point to another of the surface and address power conservation within a passive design. Simple forms of nonlocality, based on auxiliary evanescent waves [23] and leaky modes [24], have been proposed to address these needs, showing realistic pathways towards efficiencies close to unitary. However, in these cases the metasurface design process is not straightforward and typically a structure optimization is necessary to push the efficiency close to unitary. Bi-anisotropic meta-gratings have also been proposed for electromagnetics [25]-[28] and acoustics [29], which introduce an effective form of nonlocality in each unit cell exploiting resonant scattering and asymmetries. While unitary efficiency can be achieved with these passive structures within a simple implementation, still optimization to suppress the undesired scattering orders is required in practical designs, and beam steering to arbitrary angles may require complicated unit cell designs.

While acoustic unitary transmission metasurfaces have been recently proposed both in theory [17] and experiments [30] using bi-anisotropic unit cells, acoustic reflection metasurfaces with large efficiency have been reported in a small number of instances, because of the mentioned challenges [31]. Ref. [17] reported 95% reflection efficiency through numerical optimization of the metasurface structure, while Ref. [31] realized 97% reflection relying on a nonplanar surface. In this paper, we explore suitably engineered nonlocality in acoustic unit cells to design unitary reflection acoustic metasurfaces with planar profile. Tailored nonlocal unit cells can accurately control the tunneling of energy between neighboring units, offering a simple design pathway towards efficient reflective acoustic metasurfaces without design limitations and trade-offs. Our analysis proves that the efficiency of our designed metasurfaces can reach unitary levels based on a straightforward design and an easy-to-understand physical mechanism, highlighting the

powerful opportunities enabled by engineered nonlocality in metasurface designs for wavefront transformations.

II. Limitations of Local Metasurfaces

Consider an acoustic plane wave $p_i = p_{i0} e^{ik \sin\theta_i x} e^{-ik \cos\theta_i y}$ traveling in the *x*-*y* plane with incidence angle θ_i, where p_{i0} is the complex amplitude and k is the free-space wave number. Here and in the following, the time convention $e^{-i\omega t}$ is omitted for simplicity. We aim to design a planar metasurface lying on the *x*-*z* plane, steering the impinging wavefront in reflection towards the angle θ_r, with pressure $p_r = p_{r0} e^{ik \sin\theta_r x} e^{ik \cos\theta_r y}$, as shown in Fig. 1(a). For unitary reflection, energy conservation requires $p_{r0} = p_{i0} \sqrt{\cos\theta_i / \cos\theta_r}$. In a conventional gradient metasurface design, each unit cell is composed of locally vibrating elements. The right panel in Fig. 1(a) presents the equivalent circuit model for this geometry, with a single unit cell drawn in the blue dashed frame. The current source represents the net volume velocity flowing into the unit cell due to the contribution of incident and reflected waves. The impedance element $Z = -iX_2$ represents the response of the local element, which is tuned transversely element by element to provide the required phase gradients to steer the wave. This circuit model describes all designs for metasurfaces based on local approaches, no matter whether the realization is based on folded units [12] or Helmholtz resonators [13]. The common drawback of these elements is obvious: each unit cell is separate from each other, which makes transverse energy tunneling between neighboring cells impossible. For passive and lossless elements, X_2 must be real. However, in order to get unitary reflection, the impedance needs to locally satisfy

$$\frac{-iX_2}{\rho_0 c_0}=\frac{\left(\cos\theta_i-\cos\theta_r\right)\cos\left(k\left(\sin\theta_r-\sin\theta_i\right)x\right)+i\left(\cos\theta_i+\cos\theta_r\right)\sin\left(k\left(\sin\theta_r-\sin\theta_i\right)x\right)}{\sqrt{\cos\theta_i\cos\theta_r}\left(\cos\theta_i+\cos\theta_r\right)-2\cos\theta_i\cos\theta_r\cos\left(k\left(\sin\theta_r-\sin\theta_i\right)x\right)} \quad (1)$$

Figure 1(b) presents the impedance distribution for a unitary local metasurface according to Eq. (1). Here the incident angle is $\theta_i=0^\circ$ and the reflection angle is $\theta_r=75.5^\circ$, and $D=2\pi/\left(\sin\theta_r-\sin\theta_i\right)$ is the period. From Eq. (1) and Fig. 1(b), it is clear that for anomalous reflection ($\theta_i\neq\theta_r$), the required impedance to provide unitary reflection is necessarily active and/or lossy, (i.e., X_2 needs to generally be a complex number) [15]. Figure 1(c) provides the distribution of Poynting vector in the *y*-direction (I_y) along the metasurface. In part of the unit cell area, the Poynting vector is negative, indicating that the energy is being absorbed by the surface, while in other areas the Poynting vector is positive, indicating that energy is being emitted. Eq. (1) essentially forbids unitary reflection with passive and lossless local metasurfaces.

III. Nonlocal Metasurfaces

In order to realize unitary reflection avoiding the use of active and/or lossy unit cells, we propose the use of engineered nonlocality in the unit cells, which therefore support transverse tunneling of energy from some regions of the surface to others, mimicking effective active and lossy unit cells, as shown in Fig. 2(a). In acoustics, we can implement this idea by opening a physical path between neighboring unit cells, supporting flows of pressure or velocity. In the equivalent circuit, this extra path can be modeled as an extra series impedance element $-iX_1$ connecting transversely neighboring unit cells, as shown in the right panel of Fig. 2(a). Our goal is to use only passive elements with engineered nonlocality to realize unitary reflection by energy tunneling, therefore X_1 and X_2 must be real.

Suppose that the length of the channel connecting neighboring elements is w, then the volume velocity through this channel is $U(x)=v(x)w\Delta z$, where Δz indicates its width in the z-direction. Mass conservation requires that the input volume velocity equals the output one, $U_{-}(x)+v_n(x)\Delta S=U_{+}(x)$, where $v_n(x)\Delta S=v_n(x)\Delta x\Delta z$ indicates the injected volume velocity contributed by incident and reflected waves. The equivalent of Kirchhoff's laws for the lumped elements $-iX_1$ and $-iX_2$ can be written as $p_t(x)=p_t(x+\Delta x)-iX_1(x)U_{+}(x)$ and $p_t(x)=-iX_2(x)\left[U_{+}(x-\Delta x)-U_{-}(x)\right]$, respectively. From these equations, we can derive the expression for the pressure along the surface as (Appendix A)

$$p_t=-\frac{i}{\bar{Y}_2}v_n+\frac{i\omega\rho_0}{\bar{Y}_2}\frac{\partial\left(\bar{Y}_1 v_x\right)}{\partial x}. \tag{2}$$

Here, $\bar{Y}_1=\dfrac{\Delta x}{X_1\Delta z}$ and $\bar{Y}_2=\dfrac{1}{\Delta x\Delta z X_2}$ are effective admittance elements, which are real because X_1 and X_2 are real in the lossless limit. In the local scenario, $X_1\to\infty$ ($Y_1\to 0$), the pressure along the surface is only proportion to the normal velocity ($p_t=-iv_n/\bar{Y}_2$), thus the metasurface converges to the conventional local surface shown in Fig. 1(a). The ratio of local pressure and velocity, i.e., the surface impedance, can thus be calculated as $Z=-i/\bar{Y}_2$. When nonlocality is considered, however, the surface pressure is no longer a monotropic function of the normal velocity v_n, but also a function of tangential velocity v_x, as shown in Eq. (2). Hence, we can calculate the Poynting vector along y as

$$I_y=\frac{1}{2}\mathrm{Re}\left(p_t v_n^{*}\right)=-\frac{\left|v_n\right|^2}{2}\mathrm{Re}\left(\frac{i}{\bar{Y}_2}\right)+\frac{1}{2}\mathrm{Re}\left(\frac{i\omega\rho_0}{\bar{Y}_2}\frac{\partial\left(\bar{Y}_1 v_x\right)}{\partial x}v_n^{*}\right). \tag{3}$$

The first term in this expression stems from the local interactions, while the second term is due to the transverse energy tunneling between unit cells. For local metasurfaces ($Y_1 \to 0$), passive and lossless units (Y_2 is real), $I_y = 0$ is always satisfied. However, for nonlocal passive and lossless metasurface (both Y_1 and Y_2 real), even though the first term of Eq. (3) is zero, the second term is nonzero, indicating an effective 'absorption' or 'radiation' of energy locally along the metasurface, based on nonlocal effects.

For given incident and reflection angles, we can evaluate the required total pressure field p_t, tangential velocity v_x and normal velocity field v_n on the metasurface. By further requiring a lossless response, we find the expression for the effective admittances $\overline{Y}_1$ and $\overline{Y}_2$ to realize unitary reflection with a passive nonlocal metasurface. The full analytical expressions as a function of incident and reflection angles are explicitly given in Appendix B. Besides beam steering, this design approach can be generalized to arbitrary wave transformations, by plugging in the equations the incident and desired reflected field distributions. By engineering the local and nonlocal impedance along the surface it is possible to transform with unitary efficiency and large flexibility the impinging sound wave in arbitrary scenarios.

IV. Unitary Reflection

As an example, we assume that the incident angle is normal to the metasurface $\theta_i = 0^\circ$ and the desired reflection angle is $\theta_r = 75.5^\circ$ ($\cos\theta_r = \frac{1}{4}$, $\sin\theta_r = \frac{\sqrt{15}}{4}$). The effective admittance can be expressed as (see detailed derivation in Appendix B)

$$\bar{Y}_1 = \frac{4\sin\left(\sin\theta_r kx\right)}{5k^2\rho_0 c_0\left[2+\cos\left(\sin\theta_r kx\right)\right]} \tag{4}$$

$$\bar{Y}_2 = -\frac{\left[7+2\cos\left(\sin\theta_r kx\right)\right]\sin\left(\sin\theta_r kx\right)}{2\rho_0 c_0\left[2+\cos\left(\sin\theta_r kx\right)\right]^2}. \tag{5}$$

Figures 2(b) and (c) show the profile of the required $\bar{Y}_1$ and $\bar{Y}_2$ to achieve unitary efficiency. In the left half period, the effective admittances are respectively negative and positive, and in the right half period, they reverse signs. By replacing Eq. (4) and (5) into Eq. (3), we find the Poynting vector profile, which coincides with the one shown in Fig. 1(c), confirming the ideal response of the surface, and its effective absorption and re-radiation across each unit cell, which is enabled in a locally lossless metasurface based on nonlocal phenomena.

In order to explore a practical realization of these concepts, we need to discretize the profile of the required admittances, and determine an acoustic micro-structure that synthesizes the nonlocal response. While the profile of $\bar{Y}_2$ has different signs in different locations, the corresponding micro-structure can be designed with folded structures [12] or Helmholtz resonators [32]-[33], consistent with previous approaches to local metasurfaces. Here we choose impedance tubes with different lengths, as shown in the inset of Fig. 2(a).

The design of the admittance $\bar{Y}_1$ is trickier, especially when the profile is negative in some portion of each unit cell. While membranes are the most common tool to provide compact

capacitive responses for sound [34]-[36], the required pretension process of each membrane makes the realization of arrays of them for metasurfaces difficult to reproduce and scale up. For this reason, we aim at using impedance tubes, which ensure stability and accuracy of implementation. However, as shown in the equivalent circuit of Fig. 2(a), the volume velocity at both sides of $\overline{Y}_1$ should be identical, but the pressure across it should not be zero. Thus, a single tube cannot realize our goal. In our realization, we use two narrow tubes connecting a wide tube to realize the required additional tunneling path, as shown in the inset of Fig. 2(a). By accurate design, the middle tube can store some of the volume velocity, which ensures that the volume velocity at both sides of $\overline{Y}_1$ is identical. This tube design can therefore synthesize either a capacitive or inductive response by changing the tube length (Appendix C).

We first discretize the required admittance profile into fourteen segments for each period. For a normally incident plane wave with desired 75.5 deg reflection angle, an efficiency of 99.6% is obtained, as shown in the left panel in Fig. 3(a). The numerical simulation is calculated by the commercial finite element method software COMSOL Multiphysics [37]. The reflection pressure field is twice stronger than the incident field, confirming unitary anomalous reflection of our metasurface. As a comparison, we remove the tunneling path, suppressing the engineered nonlocal response, and the reflection efficiency drastically decreases, while strong parasitic waves arise, as seen in the right panel in Fig. 3(a). This comparison confirms the effectiveness of our nonlocal metasurface design. Fig. 3(c) presents the schematic geometry of each unit. Here w=0.5 mm and α=3. Other design parameters can be found in Table I. We also provided the incident and reflected wave calculated by effective impedance theory shown in Fig. 3(d) for comparison.

Fig. 3(b) presents the same design with only four discrete segments in each period, i.e., a sparse discretization of the required nonlocal impedance profile. Here w=1.75 mm and α=3. Other design parameters can be found in Table II. The reflection field for the nonlocal metasurface and for the associated local profile are shown in the left and right panels, respectively. In this case, the nonlocal efficiency is still very large, 96.4%, while the local metasurface has a much poorer performance, proving the robustness of nonlocal metasurfaces to coarse discretization.

V. Conclusion

In this paper we introduced an approach to realize low-profile planar metasurfaces with unitary efficiency in acoustic wavefront transformation using engineered nonlocality. The nonlocal effect is realized by introducing a connecting path between neighboring unit cells, so that the energy can tunnel through, and synthesize effective loss and gain profiles in the effective local description of the surface. In Appendix D, we consider the presence of viscous and thermal loss in the involved materials, showing that the phenomenon is rather robust to imperfections. Different from other approaches, our design does not require engineering additional reactive fields in the proximity of the surface, and it is directly based on an analytical approach with simple design guidelines. In its actual acoustic implementation, we considered a meandering tube to synthesize the required local and nonlocal impedance profile, achieving high efficiencies even in coarsely discretized impedance profiles. Although this approach is proposed in the field of acoustics, similar approaches may be explored in electromagnetics, optics and for elastic waves, with interesting opportunities in a wide range of applications. In the paper we focused our

attention on the canonical problem of beam steering, but the analysis can be straightforwardly extended to other wavefront transformations, such as for focusing or beam multiplexing.

ACKNOWLEDGMENTS

This work was partially supported by the National Science Foundation.

APPENDIX A. I. Derivation of Nonlocal Impedance

According to Fig. 2(a), the mass conversation law and impedance relation for $-iX_1$ and $-iX_2$ can be expressed as

$$v_{-}(x)w\Delta z + v_n(x)\Delta x\Delta z = v_{+}(x)w\Delta z \tag{A1}$$

$$p_t(x) = p_t(x+\Delta x) - iX_1(x)v_{+}(x)w\Delta z \tag{A2}$$

$$\frac{p_t(x)}{-iX_2(x)} = v_{+}(x-\Delta x)w\Delta z - v_{-}(x)w\Delta z \tag{A3}$$

Substituting Eq. (A1) into Eq. (A3), we get

$$\frac{p_t(x)}{i\Delta x\Delta z X_2(x)} + v_n(x) = w\frac{\partial v_{+}(x)}{\partial x} \tag{A4}$$

Set $\overline{Y}_2(x) = \dfrac{1}{\Delta x\Delta z X_2(x)}$, Eq. (A4) is changed to

$$-ip_t(x)\overline{Y}_2(x) + v_n(x) = w\frac{\partial v_{+}(x)}{\partial x}\ . \tag{A5}$$

From Eq. (A2), we get

$$\frac{\partial p_t(x)}{\partial x} = i\frac{X_1(x)\Delta z}{\Delta x}v_{+}(x)w. \tag{A6}$$

Set $\overline{Y}_1(x)=\dfrac{\Delta x}{X_1(x)\Delta z}$, Eq. (A6) becomes

$$-i\overline{Y}_1(x)\frac{\partial p_t(x)}{\partial x}=v_+(x)w, \tag{A7}$$

And after taking the derivative in x, we get

$$w\frac{\partial v_+(x)}{\partial x}=-i\frac{\partial \overline{Y}_1(x)}{\partial x}\frac{\partial p_t(x)}{\partial x}-i\overline{Y}_1(x)\frac{\partial^2 p_t(x)}{\partial^2 x}. \tag{A8}$$

Replacing Eq. (A8) into Eq. (A5):

$$p_t(x)\overline{Y}_2(x)=\frac{\partial p_t(x)}{\partial x}\frac{\partial \overline{Y}_1(x)}{\partial x}+\frac{\partial^2 p_t(x)}{\partial^2 x}\overline{Y}_1(x)-iv_n(x) \tag{A9}$$

Note that $\dfrac{\partial p_t(x)}{\partial x}=i\omega\rho_0 v_x(x)$. Then we are able to get the pressure expression along the metasurface from Eq. (A9):

$$p_t(x)=-\frac{i}{\overline{Y}_2(x)}v_n(x)+\frac{i\omega\rho_0}{\overline{Y}_2(x)}\frac{\partial\left[\overline{Y}_1(x)v_x(x)\right]}{\partial x}. \tag{A10}$$

APPENDIX B: Derivation of Effective Admittance Profiles

Substituting the expressions of total pressure field along the metasurface $p_t=p_0e^{ik\sin\theta_i x}+p_0\sqrt{\cos\theta_i/\cos\theta_r}e^{ik\sin\theta_r x}$, total tangential velocity $v_x(x)=\dfrac{1}{i\omega\rho_0}\dfrac{\partial p_t(x)}{\partial x}$ and the total normal velocity field along the metasurface $v_n=\left(p_0\cos\theta_i/\rho_0c_0\right)e^{ik\sin\theta_i x}-\left(p_0\cos\theta_r/\rho_0c_0\right)\sqrt{\cos\theta_i/\cos\theta_r}e^{ik\sin\theta_r x}$ into Eq. (2), we get

$$\left(1+\sqrt{\frac{\cos\theta_i}{\cos\theta_r}}e^{ik(\sin\theta_r-\sin\theta_i)x}\right)\overline{Y}_2+k^2\left(\sin^2\theta_i+\sin^2\theta_r\sqrt{\frac{\cos\theta_i}{\cos\theta_r}}e^{ik(\sin\theta_r-\sin\theta_i)x}\right)\overline{Y}_1$$

$$=ik\left(\sin\theta_i+\sin\theta_r\sqrt{\frac{\cos\theta_i}{\cos\theta_r}}e^{ik(\sin\theta_r-\sin\theta_i)x}\right)\frac{\partial\overline{Y}_1}{\partial x}+i\frac{\cos\theta_r}{\rho_0c_0}\sqrt{\frac{\cos\theta_i}{\cos\theta_r}}e^{ik(\sin\theta_r-\sin\theta_i)x}-i\frac{\cos\theta_i}{\rho_0c_0} \quad \text{(B1)}$$

Note that $\overline{Y}_1$ and $\overline{Y}_2$ are real, due to the use of passive lossless units, hence we can separate Eq. (B1) into real part and imaginary part, respectively:

$$\left(1+\sqrt{\frac{\cos\theta_i}{\cos\theta_r}}\cos\left[k(\sin\theta_r-\sin\theta_i)x\right]\right)\overline{Y}_2+k^2\left(\sin^2\theta_i+\sin^2\theta_r\sqrt{\frac{\cos\theta_i}{\cos\theta_r}}\cos\left[k(\sin\theta_r-\sin\theta_i)x\right]\right)\overline{Y}_1$$

$$=-k\sin\theta_r\sqrt{\frac{\cos\theta_i}{\cos\theta_r}}\sin\left[k(\sin\theta_r-\sin\theta_i)x\right]\frac{\partial\overline{Y}_1}{\partial x}-\frac{\cos\theta_r}{\rho_0c_0}\sqrt{\frac{\cos\theta_i}{\cos\theta_r}}\sin\left[k(\sin\theta_r-\sin\theta_i)x\right] \quad \text{(B2)}$$

$$\sqrt{\frac{\cos\theta_i}{\cos\theta_r}}\sin\left[k(\sin\theta_r-\sin\theta_i)x\right]\overline{Y}_2+k^2\sin^2\theta_r\sqrt{\frac{\cos\theta_i}{\cos\theta_r}}\sin\left[k(\sin\theta_r-\sin\theta_i)x\right]\overline{Y}_1=$$

$$k\left(\sin\theta_i+\sin\theta_r\sqrt{\frac{\cos\theta_i}{\cos\theta_r}}\cos\left[k(\sin\theta_r-\sin\theta_i)x\right]\right)\frac{\partial\overline{Y}_1}{\partial x}+\frac{\cos\theta_r}{\rho_0c_0}\sqrt{\frac{\cos\theta_i}{\cos\theta_r}}\cos\left[k(\sin\theta_r-\sin\theta_i)x\right]-\frac{\cos\theta_i}{\rho_0c_0}$$

(B3)

By solving these two differential equations, we are able to uniquely determine the profile of $\overline{Y}_1$ and $\overline{Y}_2$ for arbitrary incident and reflection angles as

$$\overline{Y}_1k^2\rho_0c_0=-\frac{\sin[k(\sin\theta_i-\sin\theta_r)x]}{\left(\cos\theta_i+\cos\theta_r\right)\cos[k(\sin\theta_i-\sin\theta_r)x]+\dfrac{\cos\left(\theta_i+\theta_r\right)+1}{\sqrt{\cos\theta_i\cos\theta_r}}} \quad \text{(B4)}$$

$$\bar{Y}_2\rho_0 c_0 = \frac{\sqrt{\cos\theta_i\cos\theta_r}\,\sin\left[k(\sin\theta_i-\sin\theta_r)x\right]}{\left(1+\sqrt{\frac{\cos\theta_i}{\cos\theta_r}}\cos\left[k(\sin\theta_i-\sin\theta_r)x\right]\right)}$$

$$+\frac{\sin[k(\sin\theta_i-\sin\theta_r)x]\left(\sin^2\theta_i+\sin^2\theta_r\sqrt{\frac{\cos\theta_i}{\cos\theta_r}}\cos\left[k(\sin\theta_i-\sin\theta_r)x\right]\right)}{\left(1+\sqrt{\frac{\cos\theta_i}{\cos\theta_r}}\cos\left[k(\sin\theta_i-\sin\theta_r)x\right]\right)\left[\left(\cos\theta_i+\cos\theta_r\right)\cos[k(\sin\theta_i-\sin\theta_r)x]+\frac{\cos\left(\theta_i+\theta_r\right)+1}{\sqrt{\cos\theta_i\cos\theta_r}}\right]}$$

$$-\frac{\sin\theta_r\sqrt{\frac{\cos\theta_i}{\cos\theta_r}}\sin\left[k(\sin\theta_i-\sin\theta_r)x\right](\sin\theta_i-\sin\theta_r)\left[\cos\theta_i+\cos\theta_r+\frac{\cos\left(\theta_i+\theta_r\right)+1}{\sqrt{\cos\theta_i\cos\theta_r}}\cos[k(\sin\theta_i-\sin\theta_r)x]\right]}{\left(1+\sqrt{\frac{\cos\theta_i}{\cos\theta_r}}\cos\left[k(\sin\theta_i-\sin\theta_r)x\right]\right)\left[\left(\cos\theta_i+\cos\theta_r\right)\cos[k(\sin\theta_i-\sin\theta_r)x]+\frac{\cos\left(\theta_i+\theta_r\right)+1}{\sqrt{\cos\theta_i\cos\theta_r}}\right]^2} \tag{B5}$$

APPENDIX C. Detailed Nonlocal Metasurface Design Approach

The design structure of the nonlocal metasurface is shown in Fig. 3(c). In each unit cell, we have one left impedance tube and one right cascading tube. The left impedance tube corresponds to the traditional metasurface design and the cascading tube connecting the neighboring elements is the extra path that allows transverse energy tunneling.

For the traditional impedance with length l_0, its corresponding impedance expression is

$$\bar{Y}_2\rho_0 c_0 = -\tan kl_0 . \tag{C1}$$

Therefore, for a given admittance $\bar{Y}_2$, the desired length l_0 can be chosen as

$$l_0 = \frac{\pi - \arctan\left(\bar{Y}_2\rho_0 c_0\right)}{k} . \tag{C2}$$

The cascading tube contains two small tubes with identical width *w* and length *h* and one large tube with width αw and length *d*. Here α is the proportionality coefficient. Suppose the pressure field and velocity field in the left small tube to be $p_L = Ae^{iky} + Be^{-iky}$ and $v_L = \left(Ae^{iky} - Be^{-iky}\right)/\rho_0 c_0$, respectively. And the pressure field and velocity field in the right small tube to be: $p_R = Ce^{iky}$ and $v_R = Ce^{iky}/\rho_0 c_0$, respectively. If we set the location of connection point of the small and large tubes to be *y*=0, we can also get the pressure and velocity field for the large tube: $p_{Large} = Ee^{iky} + Ee^{-2ikd}e^{-iky}$ and $v_{Large} = \left(Ee^{iky} - Ee^{-2ikd}e^{-iky}\right)/\rho_0 c_0$. At the connection point *y*=0, the pressure should be continuous:

$$A + B = C = E + Ee^{-2ikd}. \tag{C3}$$

At the same point, the mass conservation law requires

$$w\frac{A-B}{\rho_0 c_0} + w\frac{C}{\rho_0 c_0} = \alpha w\frac{E - Ee^{-2ikd}}{\rho_0 c_0}. \tag{C4}$$

In addition, the input and outgoing velocities at the left and right small tube need to be identical:

$$\frac{Ae^{ikh} - Be^{-ikh}}{\rho_0 c_0} = -\frac{Ce^{ikh}}{\rho_0 c_0}. \tag{C5}$$

The impedance relation for $\bar{Y}_1$ requires

$$Ae^{ikh} + Be^{-ikh} = Ce^{ikh} - i\frac{w\Delta x}{\bar{Y}_1}\left(\frac{Ae^{iky} - Be^{-iky}}{\rho_0 c_0}\right). \tag{C6}$$

Combining Eqs. (C3)-(C6), we can get the required length of *h* and *d* for any admittance $\bar{Y}_1$ as

$$d = \frac{\pi + \arctan\left(\dfrac{2\alpha w \Delta x \rho_0 c_0 \overline{Y}_1}{\left(w\Delta x\right)^2 - \left(\alpha \rho_0 c_0 \overline{Y}_1\right)^2} \right)}{2k} \tag{C7}$$

$$h = \frac{\pi + \arctan\left(\dfrac{4 w \Delta x \rho_0 c_0 \overline{Y}_1}{\left(2\rho_0 c_0 \overline{Y}_1\right)^2 - \left(w\Delta x\right)^2} \right)}{2k}. \tag{C8}$$

APPENDIX D. Viscous phenomena and thermal loss

We have explored the effect of realistic loss for the design shown in Fig. 3b by taking the viscous effects into consideration. The simulation including realistic viscous and thermal loss is performed through COMSOL Multiphysics Thermoviscous Acoustics Model. In our simulation, we choose air as the background medium and set thermal conductivity $k = 0.025768\ W/(m \cdot K)$, dynamic viscosity $\mu_B = 1.814 \times 10^{-5}\ Pa \cdot s$, bulk viscosity $\mu_B = 1.0884 \times 10^{-5}\ Pa \cdot s$. The boundary conditions are set to 'no slip' for the mechanical boundary value problem, and to isothermal for the thermal one. While the efficiency of beam steering is slightly deteriorated because of the small width of the considered channels, we envision a trade-off between channel width to impart the nonlocal effect (and hence metasurface thickness), and overall efficiency of wavefront transformation.

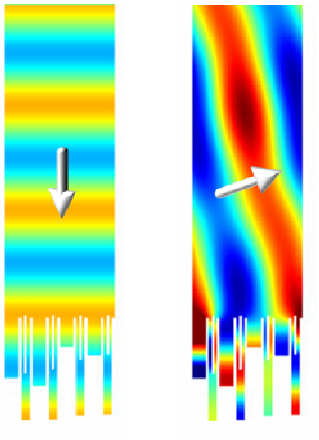

Fig. D. Simulation result for the design shown in Fig. 3(b) by taking viscous effects and thermal loss into consideration.

References

[1] N. M. Estakhri, and A. Alu, Recent progress in gradient metasurfaces, *J. Opt. Soc. Am. B* **33**, A21 (2016).

[2] H. T. Chen, A. J. Talor, and N. Yu, A review of metasurfaces: physics and applications, *Rep. Prog. Phys.* **79,** 076401 (2016).

[3] B. Assouar, B. Liang, Y. Wu, Y. Li, J.-C. Cheng, and Y. Jing, Acoustic metasurfaces, *Nat. Rev. Mater.* **3**, 460-472 (2018).

[4] Y. Tian, Q. Wei, Y. Cheng, and X. Liu, Acoustic holography based on composite metasurface with decoupled modulation of phase and amplitude, *Appl. Phys. Lett.* **110**, 191901 (2017).

[5] Y. Cheng, C. Zhou, B. G. Yuan, D. J. Wu, Q. Wei, and X. J. Liu, Ultra-sparse metasurface for high reflection of low-frequency sound based on artificial Mie resonances, *Nat. Mater.* **14**, 1013 (2015).

[6] N. Yu, P. Genevet, M. A. Kats, F. Aieta, J. P. Tetienne, F. Capasso, and Z. Gaburro, Light propagation with phase discontinuities: generalized laws of reflection and refraction, *Science* **334**, 333 (2011).

[7] A. V. Jildishev, A. Boltasseva, and V. M. Shalaev, Planar photonics with metasurfaces, *Science* **339**, 1232009 (2013).

[8] F. Monticone, N. M. Estakhri, and A. Alu, Full control of nanoscale optical transmission with a composite metascreen, *Phys. Rev. Lett.* **110,** 203903 (2013).

[9] N. M. Estakhri, and A. Alu, Manipulating optical reflections using engineered nanoscale metasurfaces, *Phys. Rev. B* **89,** 235419 (2014).

[10] S. Sun, Q. He, S. Xiao, Q. Xu, X. Li, and L. Zhou, Gradient-index meta-surfaces as a bridge linking propagating waves and surface waves, *Nat. Mater.* **11**, 426 (2012).

[11] Y. Xie, W. Wang, H. Chen, A. Konneker, B. I. Popa and S. A. Cummer, Wavefront modulation and subwavelength diffractive acoustic with an acoustic metasurface, *Nat. Commun.* **5**, 5553 (2014).

[12] Y. Li, B. Liang, Z. Gu, X. Zhou, and J. Cheng, Reflected wavefront manipulation based on ultrathin planar acoustic metasurfaces, *Sci. Rep.* **3**, 2546 (2013).

[13] Y. Li, X. Jiang, B. Liang, J. Cheng, and L. Zhang, Metascreen-based acoustic passive phased array, *Phys. Rev. Appl.* **4**, 024003 (2015).

[14] B. Yuan, Y. Cheng, and X. Liu, Conversion of sound radiation pattern via gradient acoustic metasurface with space-coiling structure, *Appl. Phys. Express* **8**, 027301 (2015).

[15] N. M. Estakhri, and A. Alu, Wave-front transformation with gradient metasurfaces, *Phys. Rev. X* **6**, 041008 (2016).

[16] V. S. Asadchy, M. Albooyeh, S. N. Tcvetkova, A. Díaz-Rubio, Y. Ra'di, and S. A. Tretyakov, Perfect control of reflection and refraction using spatially dispersive metasurfaces, *Phys. Rev. B* **94**, 075142 (2016).

[17] A. Díaz-Rubio and S. A. Tretyakov, Acoustic metasurfaces for scattering-free anomalous reflection and refraction, *Phys. Rev. B* **96**, 125409 (2017).

[18] C. Pfeiffer and A. Grbic, Metamaterial Huygens' surfaces: tailoring wave fronts with reflectionless sheets, *Phys. Rev. Lett.* **110**, 197401 (2013).

[19] A. Epstein, and G. V. Eleftheriades, Huygens' metasurfaces via the equivalence principle: design and applications, *J. Opt. Soc. Am. B* **33,** A31 (2016).

[20] M. Kim, A. M. H. Wong, and G. V. Eleftheriades, Optical Huygens' metasurfaecs with independent control of the magnitude and phase of the local reflection coefficients, *Phys. Rev. X* **4,** 041042 (2014).

[21] J. Zhao, B. Li, Z. Chen, and C. Qiu, Manipulating acoustic wavefront by inhomogeneous impedance and steerable extraordinary reflection, *Sci. Rep*. **3,** 2537 (2013).

[22] J. Zhao, B. Li, Z. N. Chen, and C. Qiu, Redirection of sound waves using acoustic metasurfaces, *Appl. Phys. Lett.* **103,** 151604 (2013).

[23] A. Epstein, and G. V. Eleftheriades, Synthesis of passive lossless metasurfaces using auxiliary fields for reflectionless beam splitting and perfect reflection, *Phys. Rev. Lett.* **117,** 256103 (2016).

[24] A. Díaz-Rubio, V. Asadchy, A. Elsakka, and S. Tretyakov, From the generalized reflection law to the realization of perfect anomalous reflectors, *Sci. Adv.* **3**, e1602714 (2017).

[25] Y. Ra'di, D. L. Sounas, and A. Alu, Metagratings: Beyond the limits of graded metasurfaces for wave front control, *Phys. Rev. Lett.* **119**, 067404 (2017).

[26] A. M. H. Wong and G. V. Eleftheriades, Perfect anomalous reflection with a bipartite huygens' metasurface, *Phys. Rev. X* **8**, 011036 (2018).

[27] M. Chen, E. Abdo-Sanchez, A. Epstein, and G. V. Eleftheriades, Theory, design, and experimental verification of a reflectionless bianisotropic Huygens' metasurface for wide-angle refraction, *Phys. Rev. B* **97**, 125433 (2018).

[28] V. Asadchy, A. Diaz-Rubio, S. Tretyakov, Bianisotropic metasurfaces: physics and applications. Nanophotonics, 7, 1069-1094 (2018).

[29] L. Quan, Y. Ra'di, D. Sounas, and A. Alu, Maximum Willis coupling in acoustic scatterers, Phys. Rev. Lett. 120, 254301 (2018).

[30] J. Li, C. Shen, A. Díaz-Rubio, S. Tretyakov, and S. Cummer, Systematic design and experimental demonstration of bianisotropic metasurfaces for scattering-free manipulation of acoustic wavefronts, Nat. Commun. 9, 1342 (2018).

[31] A. Diaz-Rubio, J. Li, C. Shen, S. A. Cummer, and S. A. Tretyakov, Power flow-conformal metamirrors for engineering wave reflections, Sci. Adv. 5, eaau7288 (2019).

[32] L. Quan, X. Zhong, X. Liu, X. Gong and P. A. Johnson, Effective impedance boundary optimization and its contribution to dipole radiation and radiation pattern control, *Nat. Commun.* **5**, 3188 (2014).

[33] L. Quan, F. Qian, X. Liu, X. Gong and P. A. Johnson, Mimicking surface plasmons in acoustics at low frequency, *Phys. Rev. B* **92**, 104105 (2015).

[34] L. Quan, F. Qian, X. Liu and X. Gong, A nonlinear acoustic metamaterial: Realization of a backwards-traveling second-harmonic sound wave, *J. Acoust. Soc. Am.* **139**, 3373-3385 (2016).

[35] R. Fleury and A. Alu, Extraordinary sound transmission through density-near-zero ultranarrow channels, *Phys. Rev. Lett.* **111**, 055501 (2013).

[36] S. H. Lee, C. M. Park, Y. M. Seo, S. G. Wang and C. K. Kim, Composite acoustic medium with simultaneously negative density and modulus, *Phys. Rev. Lett.* **104**, 054301 (2010).

[37] COMSOL Multiphysics, https://www.comsol.com.

(mm)	1	2	3	4	5	6	7
l_0	36.8	40.9	43.8	45.8	46.8	46.9	43.2
d	32.7	33.6	33.7	33.8	33.8	33.8	33.6
h	35.2	33.9	33.6	33.5	33.5	33.5	33.9
	8	9	10	11	12	13	14
l_0	25.6	21.9	22.0	23.0	25.0	27.9	32.0
d	34.5	34.2	34.2	34.2	34.3	34.4	35.3
h	32.6	32.9	33.0	32.9	32.8	32.6	31.3

TABLE I. Detailed design parameters of each unit shown in Fig. 3(a).

(mm)	1	2	3	4
l_0	40.5	45.8	20.5	25.8
d	30.1	32.9	36.6	39.0
h	37.6	34.7	28.2	25.1

TABLE II. Detailed design parameters of each unit shown in Fig. 3(b).

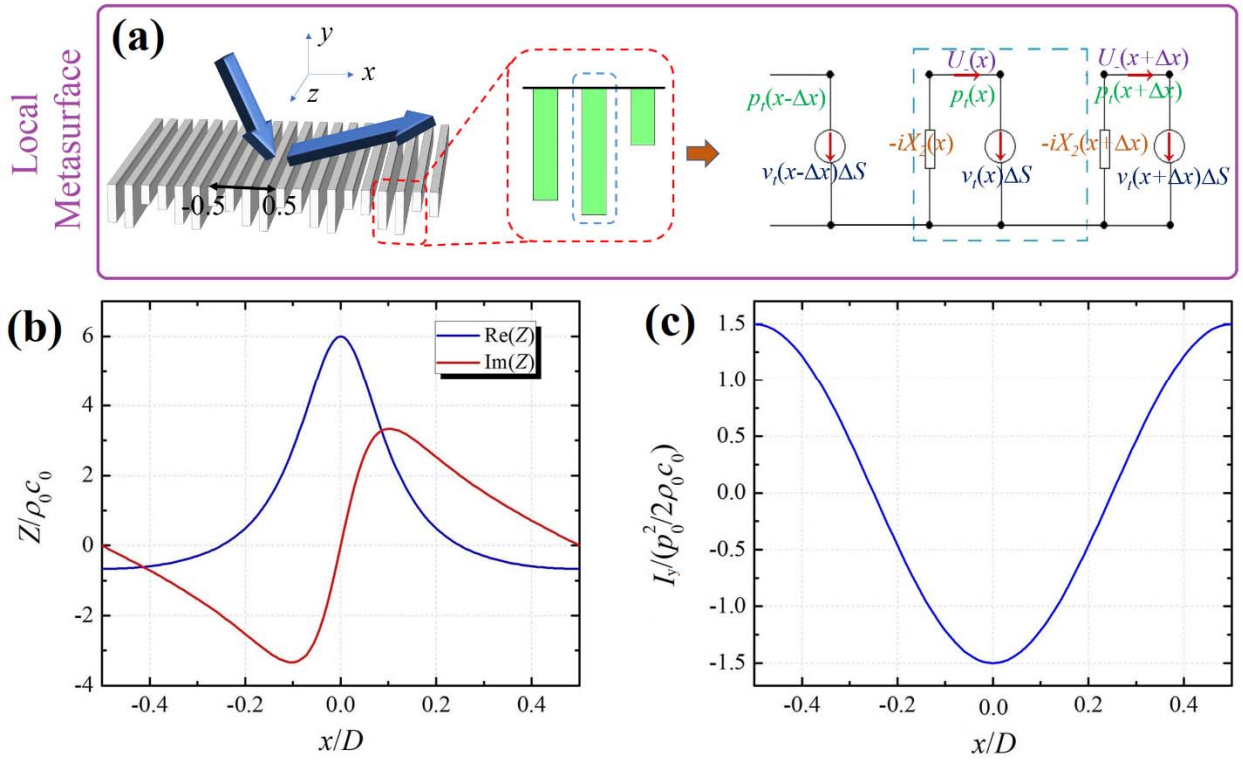

Fig. 1. (a) Schematic geometry and equivalent circuit model for a local metasurface. The blue dashed frame indicates one unit cell. The current source indicates the net volume velocity flowing into the metasurface, and the lumped impedance element models the local unit cell response. (b) Local impedance profile with the use active and/or lossy units. The required impedance is active in some areas of the unit cell and lossy in others. (c) Distribution of Poynting vector in the *y*-direction along the unit cell.

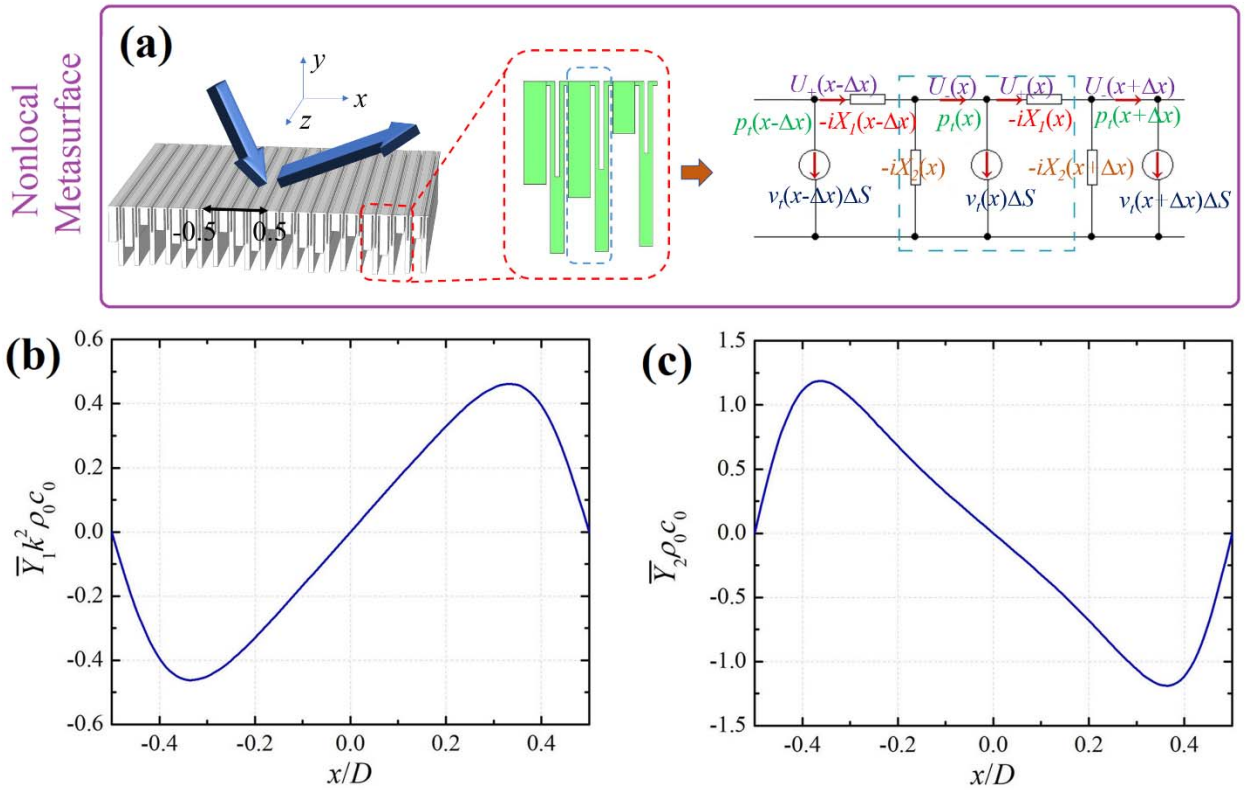

Fig. 2. (a) Schematic geometry and its equivalent circuit model for the proposed nonlocal metasurface. The equivalent circuit model introduces an extra transverse path connecting neighboring elements, and thus makes the impedance nonlocal. Energy tunnels through this path, so that unitary efficiency can be achieved with passive lossless elements. (b) Distribution of the effective series admittance $\overline{Y}_1$ to realize unitary reflection. (c) Distribution of the effective shunt admittance $\overline{Y}_2$.

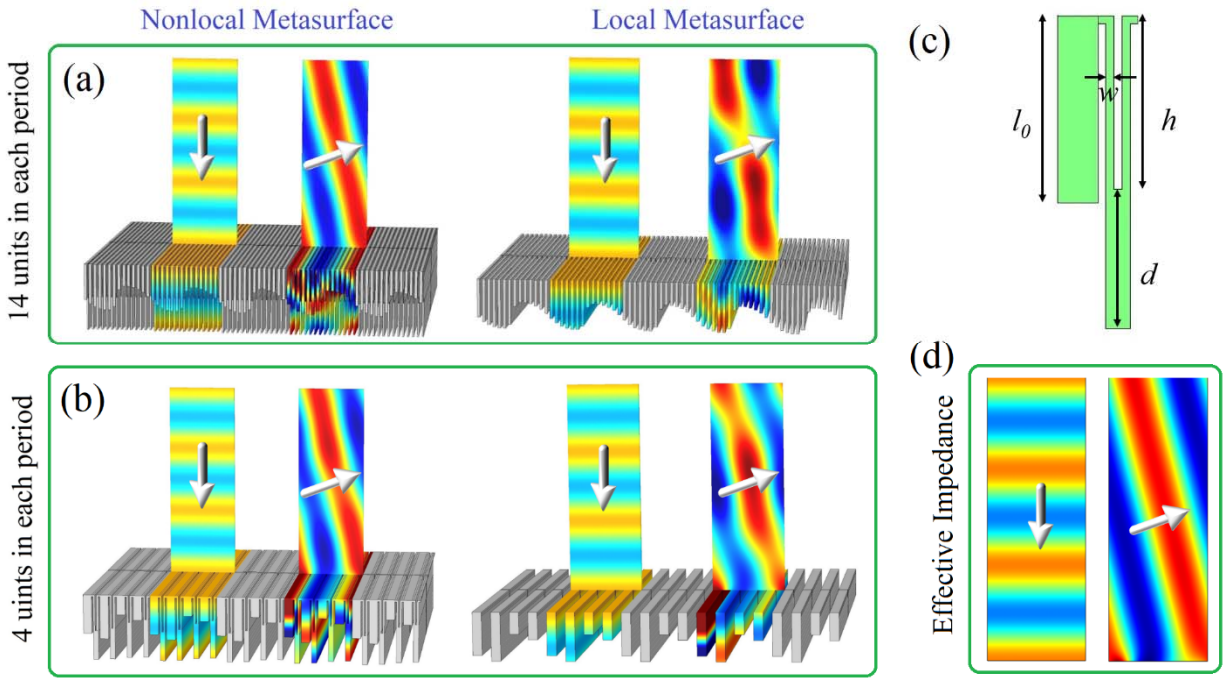

Fig. 3. (a) Discretized reflection metasurface with realistic implementation using 14 units in each period. The left panel presents the incident and reflection field for a nonlocal metasurface with connecting paths. The right panel presents the corresponding field for a local metasurface without transverse connections. For the nonlocal metasurface with 14 units in each period, the efficiency reaches 99.6%. (b) Reflection metasurface with 4 elements in each unit cell. The left and right panels present the incident wave and the reflection field for nonlocal and for local metasurface, respectively. For the nonlocal metasurface with 4 units in each period, the efficiency reaches 96.4%. (c) Schematic geometry of each unit. (d) Incident and reflected wave calculated through effective impedance theory.